

The stability of strong waves and its implications for pulsar wind shocks

Iwona Mochol* and John G. Kirk

Max-Planck-Institut für Kernphysik, Saupfercheckweg 1, 69117 Heidelberg, Germany

Received ..., accepted ...

Published online later

Key words binaries: individual (B1259-63, HESS J0632+057) – plasmas – pulsars: general – stars: winds, outflows – waves

Strong waves can mediate a shock transition between a pulsar wind and its surroundings, playing the role of an extended precursor, in which the energy is effectively transferred from fields to non-thermal particles. The damping of such precursors results in an essentially unmagnetized shock near the equator. In this context, we discuss the stability of strong waves and its implications for the properties of shocks. Those with stable precursors can exist in the winds of most of isolated pulsars, but the precursors may be unstable if the external pressure in the nebula is high, as in Vela-like pulsars. Pulsar wind shocks in eccentric binary systems, such as B1259–63, can acquire precursors only at certain orbital phases, and this process should be accompanied by enhanced synchro-Compton and inverse Compton emission from the precursor. The same scenario may be at work in the binary HESS J0632+057.

© 2006 WILEY-VCH Verlag GmbH & Co. KGaA, Weinheim

1 Introduction

The presence of electromagnetic (EM) waves of large intensity close to highly magnetized stars, has been discussed since late 1960's. Before the discovery of pulsars Pacini (1967), and later also Gunn & Ostriker (1969), suggested that a spinning neutron star emits dipole radiation at the rotational frequency, which deposits fields, energy and radial momentum in the surrounding nebula. Moreover, the emission of a test particle accelerated in the high-intensity wave closely resembles synchrotron emission in a static magnetic field, and Gunn & Ostriker (1971) attributed the continuum emission from the Crab nebula to this so-called synchro-Compton (SC) process. Rees (1971) pointed out that dipole radiation, and therefore also the SC emission, is linearly polarized at the equator, circularly polarized along the rotational axis, and elliptically polarized at other latitudes. Since the linear component has the same direction at all latitudes, the model was in agreement with the observed uniform direction of polarization in the inner nebula. A contribution from the polar regions, however, was predicted to give a few percent of circular polarization, which was not found in the optical measurements of Landstreet & Angel (1971). On the other hand, the observations excluded only the model of vacuum dipole radiation. Additionally, the model of the pulsar magnetosphere proposed by Goldreich & Julian (1969) brought into consideration prolific pair production and the existence of a plasma around a rotating neutron star. The need for a self-consistent treatment of large-amplitude electromagnetic waves propagating in plasmas (“strong waves”) was realized (Clemmow, 1974; Max & Perkins,

1971; Max, 1973). These early papers, however, showed that the propagation of such waves in the vicinity of pulsars is strongly restricted: they cannot propagate in very dense media, and, therefore, one cannot expect them close to the light cylinder. They were also shown to be very unstable (Lee & Lerche, 1978; Max & Perkins, 1972) and radiatively damped (Asseo et al., 1978).

Pulsar spin-down power and angular momentum are thought, instead, to be carried away by a relativistic wind, a mixture of a plasma and frozen-in EM fields, launched close to the light cylinder $r_L = c/\omega$. According to pulsar models, an assumed large pair production rate in the magnetosphere validates the magnetohydrodynamic (MHD) description of the wind. Far from the star, the dominant component of the magnetic field is toroidal, and the structure of the outflow is that of an entropy wave: it can be approximated by spherical current sheets, separating stripes of magnetized plasma with opposite magnetic polarity (“striped wind”). The wind is thought to power the diffuse emission of the nebula beyond the termination shock, which puts strict limits on the plasma magnetization downstream of the shock. However, according to theoretical pulsar models, the wind is highly magnetized when it is launched. Therefore, the question arises of how and where the wind dissipates its EM energy to the plasma. This so-called “ σ -problem” cannot be solved by ideal MHD, because a radial highly magnetized MHD wind does not collimate as it propagates, and, therefore, does not convert the energy from the EM fields to kinetic form, and arrives at the shock still Poynting dominated. Shocks in magnetized flows are very weak, implying that the magnetization and the flow velocity practically do not change across them. The non-oscillating component of the fields in the wind has been

* Corresponding author: e-mail: iwona.mochol@mpi-hd.mpg.de

shown to dissipate in the bulk of the nebula (Begelman, 1998; Porth et al., 2013). Therefore the problem concerns mainly the dissipation of the wave-like oscillating component of the fields. Lyubarsky (2003) has proposed a solution, in which the striped wind, due to interaction with the shock, becomes compressed and the stripes dissipate the energy by the driven magnetic reconnection. Particle-In-Cell (PIC) simulations (Sironi & Spitkovsky, 2011) show that this mechanism operates also in 2D and 3D, but in order to reproduce the observed particle spectra, a very high plasma density has to be assumed. In fact, in plasmas of the assumed densities, reconnection in the wind would start much earlier, before it arrives at the shock (Kirk & Skjæraasen, 2003).

Thus, a complementary scenario must be at work when the plasma density is below the critical value. In a radial wind, the density drops with distance, and, beyond a certain point, strong EM waves can propagate (Melatos & Melrose, 1996; Usov, 1975), both outwards from the star, and inwards from the shock. Because they have large intensities, they interact nonlinearly with each other. Instead of a superposition of outward propagating waves and reflected waves, one must search for self-consistent solutions, containing both these components, and matching the outer boundary conditions. The simplest approach is to treat this process as a mode conversion between an MHD and a self-consistent EM wave, which forms a precursor to the shock. In this precursor a significant fraction of the flow energy is transported by the particles, which provides a solution to the σ -problem in the regime of low plasma density (Arka & Kirk, 2012; Kirk, 2010). This approach is important to accurately describe the structure of shocks of isolated pulsars, as well as those in binary systems at certain orbital phases (Mochol & Kirk, 2013a). In the latter case, one can expect a shock regime switch when it becomes possible for a shock to acquire a precursor. Close to this transition point, strong waves can be very efficient emitters, providing an explanation of the peculiar flare in the binary B1259–63 (Mochol & Kirk, 2013b).

In Sect.2 we introduce the MHD pulsar wind. In Sect.3 we describe the two-fluid model of EM waves and their propagation in pulsar winds, and in Sect.4 we discuss their stability. The radiative signatures are presented in Sect.5. The implications for the shocks of isolated PWNe, the binary system B1259–63, and a new prediction for the binary HESS J0632+057 are discussed in Sect.6.

2 The MHD pulsar wind

The ability of a monochromatic, plane wave to accelerate a particle is quantified by the strength parameter: it expresses the Lorentz factor of a particle that it would gain if it were accelerated by the wave field of amplitude E from rest over one wavelength c/ω :

$$a = \frac{eE}{mc\omega} \quad (1)$$

We adapt this definition also to describe a general, nonvacuum wave. We assume that the wave carries the entire rotational power L_{sd} of the central compact object. In this case, the strength parameter at the light cylinder

$$a_L = \left(\frac{4\pi e^2 L_{sd}}{\Omega_s m^2 c^5} \right)^{1/2} = 3.4 \times 10^{10} L_{sd,38}^{1/2} (4\pi/\Omega_s) \quad (2)$$

where Ω_s is the solid angle occupied by the wind. Note that since the luminosity carried by the wind decreases with the distance from the pulsar, the strength parameter also decreases $a = a_L r_L/r$.

The particle flux density carried by the wind $J = \dot{N}/(r^2 \Omega_s)$, where \dot{N} is the pair production rate in the magnetosphere, also decreases with distance. Thus, the maximum available energy per particle in the wind is a distance-independent parameter

$$\mu = \frac{L_{sd}}{N m c^2} = \frac{a_L}{4\kappa} \quad (3)$$

where κ is the multiplicity (the ratio of the pair production rate to the Goldreich-Julian production rate), see Kirk (2010) for a definition.

The ratio of the Poynting flux to the particle energy flux carried by the wind defines the magnetization parameter σ_0 . A cold, supermagnetosonic and magnetically dominated flow has

$$1 \ll \sigma_0 \lesssim \mu^{2/3} \quad (4)$$

The radial momentum of an MHD flow is another distance independent parameter: $\nu \approx \mu - \sigma_0/(2\mu)$. Its large value, $\nu \sim \mu$, implies that the particles move almost purely radially in the wind and the magnetization stays constant up to very large distances $r \sim a_L r_L/\sigma_0$, where charge-starvation forces a significant transverse momentum component and the magnetization starts decreasing. This is important in unconfined flows, like those of blazar jets (Kirk & Mochol, 2011).

3 Strong waves

Nonlinear EM waves are exact solutions of the cold two-fluid (e^\pm) and Maxwell equations (plane waves are functions of only the phase variable). Their phase speed $\beta_{ph} > 1$ (superluminal modes), but the group speed is subluminal, $\beta_w = 1/\beta_{ph} < 1$. Large intensities ensure that the waves impart relativistic speeds on the particles within one period. Electrons and positrons have the same momenta p_{\parallel} in the direction of the wave propagation; in the plane transverse to the wave propagation they have equal but oppositely directed momenta $\pm \mathbf{p}_{\perp}$. In circularly polarized waves, the current that they generate exactly balances the displacement current of a wave $|\mathbf{p}_{\perp}| = e |\mathbf{E}|/mc\omega$.

The dispersion relation of circularly polarized electromagnetic waves in plasmas (e.g., Clemmow, 1974)

$$\omega^2 = \omega_p^2 + k^2 c^2 = \gamma_w^2 \omega_p^2 \quad (5)$$

where $\gamma_w = (1 - \beta_w^2)^{-1/2}$, implies that they can propagate only when their frequency is larger than the local plasma frequency $\omega_p = (8\pi e^2 n/m)^{1/2}$ (n is the proper density). In a pulsar wind two facts are important: (1) the frequency of an EM wave is fixed by the angular velocity of the neutron star ω and, therefore, it is convenient to measure β_w with respect to the pulsar frame in which the star is at rest; (2) according to the continuity equation, the local plasma frequency decreases with distance $\omega_p^2 \propto n \propto r^{-2}/\gamma$ (where $\gamma = (1 + p_\perp^2 + p_\parallel^2)^{1/2}$ is the particle Lorentz factor in the pulsar frame). Thus, the wave propagation condition $\omega > \omega_p$, following directly from Eq. (5), can be translated into a condition on the radius. With $\gamma \lesssim \mu$, one obtains $r > r_{\text{crit}} = a_L r_L / \mu$ and, therefore, a natural dimensionless radius is

$$R = r/r_{\text{crit}} \quad (6)$$

For the Crab, the critical radius $r_{\text{crit}} \sim 10^6 r_L$ is located well within the termination shock $r_{\text{ts}} \sim 10^9 r_L$.

Mode conversion takes place at a somewhat larger distance $r_{\text{conv}} > r_{\text{crit}}$, uniquely determined for each pulsar by the boundary conditions (pressure) in the nebula beyond the shock. To determine the wave properties at the conversion point, one has to solve the electromagnetic jump conditions, assuming that both MHD and EM modes carry the same particle, energy and radial momentum fluxes (Arka & Kirk, 2012). In the case of circular polarization the phase-averages can be dropped and, using definitions from Sect.2, these can be expressed in the form

$$J = 2cn p_\parallel \quad (7)$$

$$\mu = \left(\gamma + \frac{\beta_w \gamma_w^2 p_\perp^2}{p_\parallel} \right) \quad (8)$$

$$\nu = \left(p_\parallel + \frac{(1 + \beta_w^2) \gamma_w^2 p_\perp^2}{2p_\parallel} \right) \quad (9)$$

In fact there are two possible solutions for an EM wave, whose fluxes equal those of the MHD wind: a free escape mode, and a confined mode. We concentrate on the latter, which at the conversion point has the following properties:

$$\gamma \approx p_\perp \approx \mu/R_{\text{conv}}, \quad \gamma_w \approx (R_{\text{conv}}/8)^{1/4} \quad (10)$$

(assuming $p_\perp \gg p_\parallel$, valid everywhere except a very close neighbourhood of the cut-off point $R_{\text{conv}} = 1$).

In the spherical expansion of the flow, the waveform is plane only to the lowest-order short-wavelength approximation. The first-order correction describes the slow radial evolution of the lowest order, phase-averaged solution. For a circularly polarized wave the phase averages can be dropped and the evolution equations take the form:

$$\frac{1}{r^2} \frac{\partial}{\partial r} (r^2 n p_\parallel) = 0 \quad (11)$$

$$\frac{1}{r^2} \frac{\partial}{\partial r} \left(r^2 2n p_\parallel \gamma + \frac{r^2 \beta_w E^2}{4\pi m c^2} \right) = 0 \quad (12)$$

$$\frac{1}{r^2} \frac{\partial}{\partial r} \left(r^2 2n p_\parallel^2 + \frac{r^2 (1 + \beta_w^2) E^2}{8\pi m c^2} \right) = \frac{n p_\perp^2}{r} \quad (13)$$

The first equation immediately implies $p_\parallel = \mu \gamma_w^2 / R^2$. The other two are integrated with the initial conditions given by the jump conditions (8-9). Only the solution that starts at the confined mode branch slows down with distance and eventually stagnates at a finite pressure. It can, therefore, be matched to the surroundings (see Fig.1). We interpret it as an extended shock precursor.

In a radially propagating wave the phase averaged Lorentz factor of the particles, measured in the laboratory frame, turns out to be conserved. This can be proven for arbitrary wave polarization (Mochol & Kirk, 2013a). Thus, instead of equation (13) we can use

$$\frac{\partial}{\partial r} \gamma = 0 \quad (14)$$

This integral of motion is in fact an adiabatic invariant, and follows directly from the plasma neutrality in all reference frames related to the lab. frame by a Lorentz boost in the direction of wave propagation. It allows us to find the pressure at which a confined mode stagnates.

4 The stability of strong waves

Strong waves are intrinsically very unstable, unless they carry a transverse, phase-averaged component of the magnetic field (Asseo et al., 1980), or there is a fast streaming of the particles through the wave (Lee & Lerche, 1978; Romeiras, 1978; Skjæraasen et al., 2005). Here we consider only the second case as a stabilizing factor. A stability condition for a circularly polarized wave has been obtained by Lee & Lerche (1978):

$$p_\parallel'^2 - 2\gamma' p_\perp + p_\perp^2 > 0 \quad (15)$$

where a prime denotes the quantities measured in the frame comoving with the wave group speed. In pulsar winds relativistic streaming is a property of waves launched very close to the cut-off, $1 < R \lesssim (4/3)^{1/4}$, or very far from it, $R \gtrsim 100$ (Mochol & Kirk, 2013a). The condition (15) is shown as a shaded region in Fig.1. The group four-speed of a wave $\gamma_w \beta_w$, calculated from the jump conditions (7-9), is shown as a function of conversion radius R_{conv} (dotted line: free expansion branch, dashed: confined branch). Solid curves show the radial evolution of confined modes launched at different conversion radii (marked by a dot). Even if the wave is launched stable, it becomes unstable after propagation of $\sim 10^3$ wavelengths.

Where the wave is launched is uniquely determined by the external pressure

$$p_{\text{ext}} \approx \frac{L}{\Omega_s c r^2} = \frac{10^{-6} \mu_4^2}{R^2 P_1} \text{ dyn cm}^{-2} \quad (16)$$

where P_1 is the pulsar period in seconds, and $\mu = \mu_4 \times 10^4$. The waves launched in the outer stability zone match low pressure media like those of isolated pulsars, confined by nebulae at large distances. In the case of high-pressure

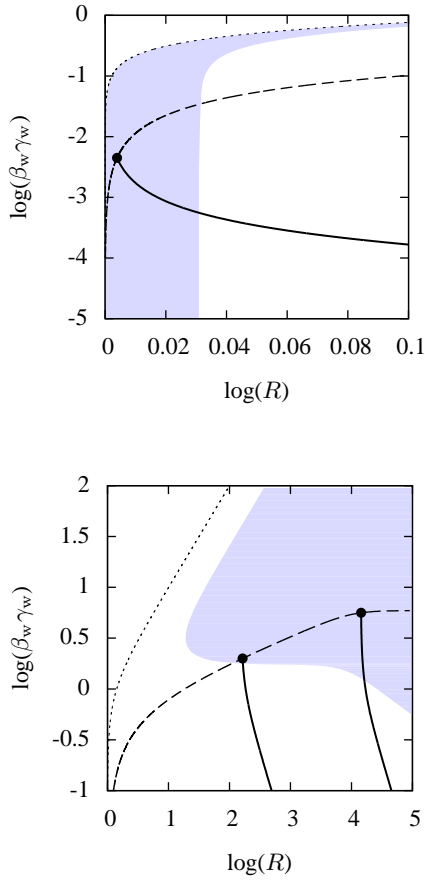


Fig. 1 Top panel: The inner zone of stability $1 < R \lesssim (4/3)^{1/4}$. Electromagnetic Hugoniot curves are plotted showing the group four-speed $\beta_w \gamma_w$ as a function of radius R_{conv} for $\mu = 10^4$, $\sigma = 100$ (dotted line: free expansion branch, dashed: confined branch). The black solid line shows the radial evolution of a wave, launched at the confined-mode branch. In the shaded region the waves are stable according to the criterion given in Eq. (15). Bottom: The outer zone of stability $R \gtrsim 100$. The same Hugoniot curves are plotted, together with two confined modes, launched at larger radius. The inner zone of stability lies close to the Hugoniot curve of the free escape mode, and is not visible on the scale of this figure.

nebulae the precursor is expected to fall into the unstable region. The waves launched in the inner stability zone match very high-pressure media like those of binaries, provided by the dense winds of their companion stars. However, in the absence of radiative damping this zone is very narrow.

5 Radiative damping

Waves launched close to the cut-off have the largest amplitudes, and, for them, radiation reaction can be an efficient mechanism of wave damping. The propagation of a wave

in a planar geometry but with radiation reaction taken into account is governed by (Mochol & Kirk, 2013b)

$$\frac{d}{dx} (np_{\parallel}) = 0 \quad (17)$$

$$\frac{d}{dx} \left(2np_{\parallel}\gamma + \frac{\beta_w E^2}{4\pi m c^2} \right) = ng^0 \quad (18)$$

$$\frac{d\gamma}{dx} = \frac{g^1 - \beta_w g^0}{2\Delta} \quad (19)$$

where $\Delta = \gamma - \beta_w p_{\parallel}$ and

$$g^{0,1} \approx -\frac{2e^4}{3m^3 c^6} E^2 |\gamma - \beta_w p_{\parallel}|^2 (\gamma, p_{\parallel}) . \quad (20)$$

One can immediately see that the ratio of changes of γ to changes of the Poynting flux per particle is $\sim p_{\parallel}^2/p_{\perp}^2 \ll 1$. Therefore, the equations suggest that the particles catalyze extraction of the Poynting flux carried by the wave, i.e., the wave energy is used to accelerate particles by exactly the amount they lose to radiation, keeping the Lorentz factor constant.

When in addition to radiation reaction IC scattering is also important, the radiative damping force acquires an additional component, $g_{\text{ic}}^{0,1}$ (see appendix A).

Importantly, the radiative signatures, i.e., the efficiency of emission $\eta = \eta_{\text{sc}} + \eta_{\text{ic}}$, defined in Eq. (A8), and the mean photon energy $\bar{x} = h\nu/mc^2$, defined in Eq. (A9) and (A10) for SC and IC processes respectively, change with the distance of the shock (see Fig.2). The overall emission efficiency in each component is an interplay between the amount of the Poynting flux available for extraction, the wave field strength (SC), and the energy density of the target photons (IC). In general, particles moving in a large-amplitude transverse wave, stay confined in the emission region longer than if they were moving purely radially.

6 Implications

6.1 PWNe

PWNe can be divided into two groups: those with stable precursors to their termination shocks and those with unstable precursors. The first group includes Crab ($R = 1355\kappa_5^{-1}$) and N158A ($R = 1540\kappa_5^{-1}$). The second includes, for instance, Vela ($R = 56\kappa_5^{-1}$), where $\kappa_5 = \kappa/(5 \times 10^5)$.

The simulations of Amano & Kirk (2013) have shown that an EM-modified shock behaves as essentially unmagnetized near the equator. The reason is that the electric field $E > B$ dominates the plasma dynamics in the EM wave, and, therefore, particle transport does not have to rely on cross field diffusion, as in a perpendicular shock. In this sense, shock mediated by a stable precursor is expected to be stronger, and, therefore, a more efficient emitter. We speculate that the nebulae with stable/unstable precursors may exhibit different radiation signatures, for instance brighter/fainter appearance. However, the quantitative analysis is difficult, because nebular emission depends

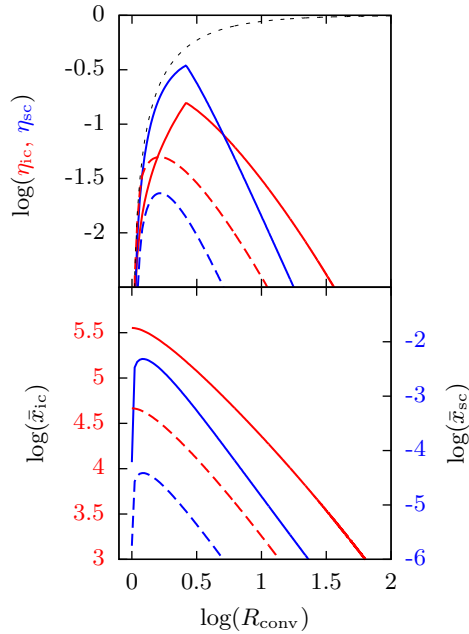


Fig. 2 Radiative signatures of the shock precursor, for different conversion radii and for $a_L = 10^{10}$, and $\gamma_{ic}/\gamma \approx 3.9$. Red: IC component, blue: SC emission. Solid: $\mu = 5 \times 10^5$, dashed $\mu = 10^5$. Black dotted line shows the available Poynting flux.

on many factors. In addition, pulsar multiplicities are unknown, although the modelling of PWNe suggests large values $\kappa \gtrsim$ a few $\times 10^5$ (Bucciantini et al., 2011).

6.2 The binary B1259–63

An interesting possibility arises in binary systems, where the shocks may switch between different regimes. When the binary members are close, such that the distance between the pulsar and the shock is smaller than the critical radius, the shock is in the MHD regime. When the separation becomes larger, a shock can acquire an EM precursor. A sudden appearance of a precursor ahead of the shock should be accompanied by enhanced emission in the SC and IC processes (see Fig.2) close to this transition point, because the precursor emission is most efficient close to the cut-off.

An example is the eccentric binary B1259–63. It consists of a pulsar on a very elongated orbit around a Be-star, with a period 3.4 years; 30 days after the periastron passage in 2010, Fermi-LAT detected a GeV flare that lasted several weeks (Abdo, 2011; Tam et al., 2011). The efficiency of this emission was extremely high, on the order of the pulsar spin-down power. This feature is challenging for all existing models: those based on electrons accelerated at the termination shock (Kong et al., 2012) have to assume strong Doppler-beaming, those based on electrons in the unshocked wind (Khangulyan et al., 2011,

2012; Pétri & Dubus, 2011) require an additional source of target photons.

The rotation period 48-ms of a pulsar implies $r_L = 2.3 \times 10^8$ cm, and spin down power $L_{sd} = 8 \times 10^{35}$ erg s^{-1} is equivalent to the strength parameter $a_L = 3 \times 10^9 (4\pi/\Omega_s)$. 30 days after periastron passage the separation between binary members is 3.7×10^{13} cm, and we assume that the shock is located roughly a mid-way between the objects. Since the flare occurs close to $R_{conv} \approx 1.5$, we obtain $\mu \sim 6 \times 10^4$ and the characteristic energy of IC photons $\epsilon_0 \sim 10$ GeV, which decreases with time.

We also expect a faint (a few $\times 10^{-3} L_{sd}$) counterpart due to synchro-Compton emission in the optical band. However, this component is swamped by photons from the luminous companion star.

In principle, an analogous, pre-periastron flare could be expected if the physical conditions at the shock were symmetric along the pulsar orbit with respect to periastron. These conditions are determined by the location of a shock between the pulsar and stellar winds, i.e., by the wind relative strength. Since the wind of the companion star is known to be highly anisotropic, the conditions at the shock are unlikely to be symmetric with respect to periastron. Therefore, a pre-periastron flare is not necessarily expected to be symmetrically timed with the post-periastron flare, and, consequently, not necessarily peaked in the same energy band.

6.3 Predictions for the binary HESS J0632+057

The recently discovered gamma-ray binary HESS J0632+057 consists of an unknown compact object on an elongated orbit (period 315 days) around a Be-star. The lightcurve exhibits enhancement of X-ray and sub-TeV emission 100 days after the periastron, and located roughly symmetrically with respect to the apastron passage (Bordas & Maier, 2012). If a binary member were a pulsar, one could expect similar behaviour as in B1259–63. The sub-TeV emission due to IC scattering of the stellar photons implies $\mu \gtrsim 3.5 \times 10^5$, and the SC emission in keV suggests the pulsar period $\lesssim 140$ ms. The maximum emission 100 days after periastron implies $a_L \approx 9 \times 10^9$.

Thus, our estimates show that the model can account for simultaneous emission in both energy bands with their unusual lightcurves (two maxima and a dip around the apastron), and predict the presence of a pulsar with period $P \lesssim 140$ ms and period derivative $\dot{P} \approx 4.4 \times 10^{-13}$.

7 Summary and conclusions

The dynamics of pulsar winds is dominated by electromagnetic fields, which, far from the star, behave more like an EM wave instead of a familiar MHD wind. These effects are crucial to a proper description of shocks in a low-density plasma, i.e., those located at large stand-off distances, $r_{ts} \gtrsim 10^2 r_{crit}$. Such shocks exhibit dissipative precursors, which modify their structure and particle accel-

ation properties. In most of the isolated pulsar winds, the precursors are stable over many wavelengths, but if the surrounding nebula is compact, like Vela, the precursors are unstable. In eccentric binaries it is possible to probe a shock regime switch between an MHD shock and an electromagnetically modified shock, and the appearance of a precursor shock can be distinguished by its radiative signatures.

Acknowledgements. IM thanks Vincent Marandon for useful discussions.

References

- Abdo, A. A. e. a. 2011, *ApJ*, 736, L11, 1103.4108
 Amano, T., & Kirk, J. G. 2013, *ApJ*, 770, 18, 1303.2702
 Arka, I., & Kirk, J. G. 2012, *ApJ*, 745, 108, 1109.2756
 Asseo, E., Kennel, C. F., & Pellat, R. 1978, *A&A*, 65, 401
 Asseo, E., Llobet, X., & Schmidt, G. 1980, *Phys. Rev. A*, 22, 1293
 Begelman, M. C. 1998, *ApJ*, 493, 291, arXiv:astro-ph/9708142
 Bordas, P. and H. E. S. S. Collaboration & Maier, G. and VERITAS Collaboration 2012, *AIP Conf. Proc.*, 1505, 366
 Bucciantini, N., Arons, J., & Amato, E. 2011, *MNRAS*, 410, 381
 Clemmow, P. C. 1974, *Journal of Plasma Physics*, 12, 297
 Goldreich, P., & Julian, W. H. 1969, *ApJ*, 157, 869
 Gunn, J. E., & Ostriker, J. P. 1969, *Nature*, 221, 454
 ——. 1971, *ApJ*, 165, 523
 Khangulyan, D., Aharonian, F. A., Bogovalov, S. V., & Ribó, M. 2011, *ApJ*, 742, 98, 1104.0211
 ——. 2012, *ApJ*, 752, L17, 1107.4833
 Kirk, J. G. 2010, *Plasma Physics and Controlled Fusion*, 52, 124029, 1008.0536
 Kirk, J. G., Ball, L., & Skjæraasen, O. 1999, *Astroparticle Physics*, 10, 31
 Kirk, J. G., & Mochol, I. 2011, *ApJ*, 729, 104, 1012.0307
 Kirk, J. G., & Skjæraasen, O. 2003, *ApJ*, 591, 366, arXiv:astro-ph/0303194
 Kong, S. W., Cheng, K. S., & Huang, Y. F. 2012, *ApJ*, 753, 127, 1205.2147
 Landstreet, J. D., & Angel, J. R. P. 1971, *Nature*, 230, 103
 Lee, M. A., & Lerche, I. 1978, *Journal of Plasma Physics*, 20, 313
 Lyubarsky, Y. E. 2003, *MNRAS*, 345, 153, arXiv:astro-ph/0306435
 Max, C., & Perkins, F. 1971, *Physical Review Letters*, 27, 1342
 ——. 1972, *Physical Review Letters*, 29, 1731
 Max, C. E. 1973, *Physics of Fluids*, 16, 1277
 Melatos, A., & Melrose, D. B. 1996, *MNRAS*, 279, 1168
 Mochol, I., & Kirk, J. G. 2013, *ApJ*, 771, 53, 1303.6434
 Mochol, I., & Kirk, J. G. 2013, accepted for publication in *ApJ*, arXiv:astro-ph/1308.0950
 Pacini, F. 1967, *Nature*, 216, 567
 Pétri, J., & Dubus, G. 2011, *MNRAS*, 417, 532, 1104.4219
 Porth, O., Komissarov, S. S., & Keppens, R. 2013, *MNRAS*, 431, L48, 1212.1382
 Rees, M. J. 1971, in *IAU Symposium*, Vol. 46, The Crab Nebula, ed. R. D. Davies & F. Graham-Smith, 407
 Romeiras, F. J. 1978, *Journal of Plasma Physics*, 20, 479
 Sironi, L., & Spitkovsky, A. 2011, *ApJ*, 741, 39, 1107.0977
 Skjæraasen, O., Melatos, A., & Spitkovsky, A. 2005, *ApJ*, 634, 542, arXiv:astro-ph/0508192
 Tam, P. H. T., Huang, R. H. H., Takata, J., Hui, C. Y., Kong, A. K. H., & Cheng, K. S. 2011, *ApJ*, 736, L10, 1103.3129

Usov, V. V. 1975, *Ap&SS*, 32, 375

A Efficiency of emission

We introduce the space-dependent magnetization parameter

$$\sigma = \frac{\beta_w p_{\perp}^2}{(8\pi e^2 n / m\omega^2) p_{\parallel} \gamma} \quad (\text{A1})$$

$$= \frac{\gamma_w^2 \beta_w p_{\perp}^2}{p_{\parallel} \gamma} \quad (\text{A2})$$

where we have used the dispersion relation for strong waves $8\pi e^2 n / m\omega^2 = 1/\gamma_w^2$ (Clemmow, 1974). This parameter allows us to express the Poynting flux per particle by $\gamma\sigma$, and the total energy per particle $\mu = \gamma(1 + \sigma)$. Eq. (18) and (19) imply that the Poynting flux decreases as

$$\frac{d}{dX} (\gamma\sigma) = -\frac{\epsilon a_L}{2\mu} \frac{\Delta p_{\perp}^2 (1 + p_{\perp}^2)}{p_{\parallel}} \quad (\text{A3})$$

where $X = x/r_{\text{crit}} = (\mu/a_L)(x/r_L)$ and $\epsilon = 2e^2\omega/3mc^3$.

One can estimate a lengthscale, on which a significant fraction of the Poynting flux is extracted

$$X_{\text{diss}} \approx \frac{2\mu}{\epsilon a_L} \left(\frac{\gamma\sigma p_{\parallel}}{\Delta p_{\perp}^2 (1 + p_{\perp}^2)} \right) \quad (\text{A4})$$

When the IC emission is important, the radiative coefficient is two-component

$$\epsilon = \epsilon_{\text{sc}} + \epsilon_{\text{ic}} \quad (\text{A5})$$

$$= \frac{2e^2\omega}{3mc^3} \left(1 + \frac{G(\gamma, x_0)\gamma_{\text{ic}}^2}{\gamma^2} \right) \quad (\text{A6})$$

where

$$\gamma_{\text{ic}} = \left(\frac{2\sigma_{\text{T}} U_{\text{rad}} c^2}{e^2 \omega^2} \right)^{1/2} \quad (\text{A7})$$

and $G(\gamma, x_0)$ is the reduction factor due to Klein-Nishina effects in the scattering of a target photon field $\nu_0 = x_0 mc^2/h$ (see, e.g., Kirk et al., 1999). A substantial fraction of the Poynting flux is converted into radiation if $X_{\text{diss}} < R_{\text{conv}}$, hence the radiation efficiency can be defined as

$$\eta = \begin{cases} \sigma/(1 + \sigma) & \text{for } X_{\text{diss}} < R_{\text{conv}} \\ \sigma R_{\text{conv}} / [X_{\text{diss}}(1 + \sigma)] & \text{for } X_{\text{diss}} > R_{\text{conv}} \end{cases} \quad (\text{A8})$$

The mean energy of radiated photons in the synchro-Compton process

$$\bar{x}_{\text{sc}}(\gamma, p_{\perp}) = 0.4\gamma^2 p_{\perp} (\hbar\omega/mc^2), \quad (\text{A9})$$

whereas the peak energy of inverse Compton scattered photons can be estimated as

$$\bar{x}_{\text{ic}}(\gamma, x_0) = (4/3)\sigma_{\text{T}} x_0 \gamma^2 G(\gamma, x_0) / \langle \dot{N}_{\gamma} \rangle, \quad (\text{A10})$$

where \dot{N}_{γ} is the scattering rate divided by the density of target photons and $\langle \dots \rangle$ indicates an angle average, see Mochol & Kirk (2013b).